

REVIEW ARTICLE

Introduction to half-metallic Heusler alloys: Electronic Structure and Magnetic Properties

I Galanakis[†], Ph Mavropoulos[‡] and P H Dederichs[‡]

[†] Materials Science Department, School of Natural Sciences, University of Patras,
Patras 265 04, Greece

[‡] Institut für Festkörperforschung, Forschungszentrum Jülich, D-52425 Jülich,
Germany

E-mail:

i.galanakis@fz-juelich.de, ph.mavropoulos@fz-juelich.de, p.h.dederichs@fz-juelich.de

Abstract. Intermetallic Heusler alloys are amongst the most attractive half-metallic systems due to the high Curie temperatures and the structural similarity to the binary semiconductors. In this review we present an overview of the basic electronic and magnetic properties of both Heusler families: the so-called half-Heusler alloys like NiMnSb and the full-Heusler alloys like Co₂MnGe. *Ab-initio* results suggest that both the electronic and magnetic properties in these compounds are intrinsically related to the appearance of the minority-spin gap. The total spin magnetic moment M_t scales linearly with the number of the valence electrons Z_t , such that $M_t = Z_t - 24$ for the full-Heusler and $M_t = Z_t - 18$ for the half-Heusler alloys, thus opening the way to engineer new half-metallic alloys with the desired magnetic properties.

PACS numbers: 75.47.Np, 71.20.Be, 71.20.Lp

Submitted to: *J. Phys. D: Appl. Phys.*

1. Half-metallic Heusler Alloys

Half-metallic ferromagnets represent a relatively new class of materials which have attracted recently a lot of interest due to their possible applications in spin electronics (also known as magnetoelectronics) [1]. In these materials the two spin bands show a completely different behaviour. While one of them (usually the majority-spin band, henceforth also referred to as spin-up band) shows a typical metallic behaviour with a nonzero density of states at the Fermi level E_F , the minority (spin-down) band exhibits a semiconducting behaviour with a gap at E_F . Therefore such half-metals can be considered as hybrides between metals and semiconductors. A schematic representation of the density of states of a normal metal, a semiconductor and a half-metal is shown in figure 1. Such half-metals exhibit, ideally, a 100% spin polarization at the Fermi level and therefore these compounds should have a fully spin-polarized current and be ideal spin injectors into a semiconductor, thus maximizing the efficiency of spintronic devices [2].

Heusler alloys [3] have attracted great interest during the last century due to the possibility to study in the same family of alloys a series of interesting diverse magnetic phenomena like itinerant and localized magnetism, antiferromagnetism, helimagnetism, Pauli paramagnetism or heavy-fermionic behavior [4, 5, 6, 7]. Recently, also their application as shape-memory alloys has been intensively discussed [8]. The first Heusler alloys studied were of the form X_2YZ and crystalize in the $L2_1$ structure which consists of four fcc sublattices, two of which are occupied by the same type of X-atoms (see figure 2). Afterwards the XYZ Heusler alloys of $C1_b$ structure were discovered, where one sublattice remains unoccupied. The latter compounds are often called half- or semi-Heusler alloys, while the $L2_1$ compounds are referred to as full Heusler alloys.

In 1983 de Groot and co-workers [9] discovered by *ab-initio* calculations that one of the half-Heusler alloys, $NiMnSb$, is half-metallic, i.e., the minority band is semiconducting with a band gap at E_F , as shown in figure 3. Since then, many other materials have also been found to be half-metallic. Besides a number of half- and full-Heusler alloys, these are some oxides (*e.g.*, CrO_2 and Fe_3O_4) [10], manganites (*e.g.*, $La_{0.7}Sr_{0.3}MnO_3$) [10], double perovskites (*e.g.*, Sr_2FeReO_6) [11], pyrites (*e.g.* CoS_2) [12], transition metal chalcogenides (*e.g.*, $CrSe$) and pnictides (*e.g.* $CrAs$) in the zinc-blende or wurtzite structures [13, 14, 15, 16], europium chalcogenides (*e.g.*, EuS) [17], and diluted magnetic semiconductors (*e.g.* Mn impurities in Si or GaAs) [18, 19]. Although thin films of CrO_2 and $La_{0.7}Sr_{0.3}MnO_3$ have been verified to present practically 100% spin-polarization at the Fermi level at low temperatures [10, 20], the Heusler alloys remain attractive for technological applications like spin-injection devices [21], spin-filters [22], tunnel junctions [23], or GMR devices [24] due to their relatively high Curie temperatures compared to other half-metallic compounds [4].

The half-metallic character of $NiMnSb$ in single crystals seems to have been well-established experimentally. Infrared absorption [25] and spin-polarized positron-annihilation [26] gave a spin-polarization of $\sim 100\%$ at the Fermi level. However, in

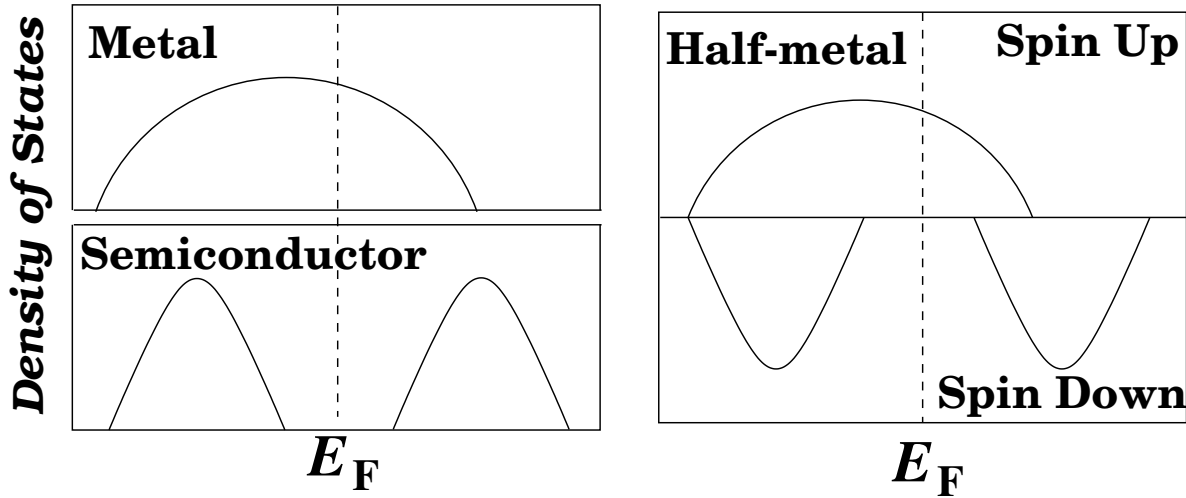


Figure 1. Schematic representation of the density of states for a half-metal with respect to normal metals and semiconductors.

many other experiments half-metallicity has not been found. In most cases the reason for this is that properties have been measured which are surface and interface sensitive. It has been shown [27, 28, 29] that near surfaces and interfaces the half-metallic property is in most cases lost. Therefore most of these experiments do not allow for conclusions about half-metallicity in the bulk to be drawn.

In this introductory review we discuss the basic electronic and magnetic properties of the half-metallic Heusler alloys. Analyzing *ab-initio* results and using group theory and simple models we explain the origin of the gap in both the half- and full-Heusler alloys as arising from *d-d* hybridisation, which is fundamental for understanding their electronic and magnetic properties. For both families of compounds the total spin magnetic moment scales with the number of valence electrons and can be described by a Slater-Pauling rule, thus opening the way to engineer new half-metallic Heusler alloys with desired magnetic properties. This behaviour is governed by the fact that in these alloys the number of minority valence electrons per unit cell is an integer given by the number of occupied minority valence bands, being equal to 9 for the half-Heusler and 12 for the full-Heusler compounds. We discuss the role of spin-orbit coupling, which in principle destroys the minority band gap, however in practice leads only to a small reduction of spin polarization. We will not discuss the effects of defects, interfaces or surfaces, for which we refer to a recent book [30] and to many papers in this issue.

In the following sections we discuss the electronic and magnetic properties of half-metallic half-Heusler compounds XYZ (Sect. 2) and of full-Heusler compounds X_2YZ (Sect. 3), in particular the origin of the minority gap and the resulting Slater-Pauling rules. Sect. 4 shortly addresses the effect of the lattice parameter, while in Sect. 5 the effect of spin-orbit coupling is investigated, reducing the spin polarization at E_F . We conclude with a summary in Sect. 6.

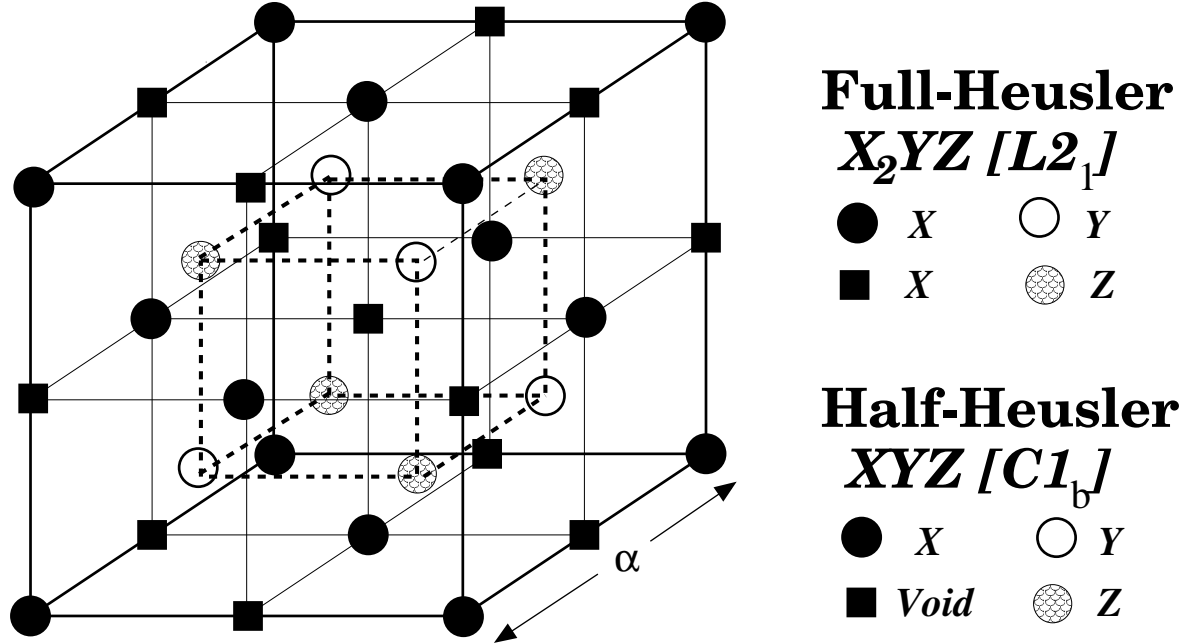


Figure 2. $C1_b$ and $L2_1$ structures adapted by the half- and full-Heusler alloys. The lattice is consisted of 4 interpenetrating fcc sublattices. The unit cell is that of a fcc lattice with four atoms as basis, *e.g.* CoMnSb: Co at $(0\ 0\ 0)$, Mn at $(\frac{1}{4}\ \frac{1}{4}\ \frac{1}{4})$, a vacant site at $(\frac{1}{2}\ \frac{1}{2}\ \frac{1}{2})$ and Sb at $(\frac{3}{4}\ \frac{3}{4}\ \frac{3}{4})$ in Wyckoff coordinates. In the case of the full Heusler alloys also the vacant site is occupied by a Co atom. Note also that if all atoms were identical, the lattice would be simply the bcc.

2. Electronic and Magnetism Properties of Half-Heusler Alloys

2.1. Band Structure of Half-Heusler Alloys

In the following we present results for some typical half-Heusler alloys of $C1_b$ structure (see figure 2). To perform the calculations, we used density-functional theory in the local density approximation (LDA) in connection with the full-potential screened Korringa-Kohn-Rostoker (FSKKR) method [31, 32]. The prototype example is NiMnSb, the half-metal discovered in 1983 by de Groot [9]. Figure 3 shows the density of states (DOS) of NiMnSb in a non-spin-polarized calculation (left upper panel) and in a calculation correctly including the spin-polarization (right panel). Given are the local contributions to the density of states (LDOS) on the Ni site (dashed), the Mn site (full line) and the Sb site (dotted). In the non-magnetic case the DOS of NiMnSb has contributions from 4 different bands: Each Sb atom with the atomic configuration $5s^25p^3$ introduces a deep lying s band, which is located at about -12eV and is not shown in the figure, and three Sb p -bands in the regions between -5.5 and -3 eV. These bands are separated by a deep minimum in the DOS from 5 Ni d bands between -3 and -1 eV, which themselves are separated by a sizeable band gap from the upper 5 d -bands of Mn. Since all atomic orbitals, *i.e.*, the Ni d , the Mn d and the Sb sp orbitals hybridise with each other, all bands are hybrids between these states, being either of bonding or antibonding type.

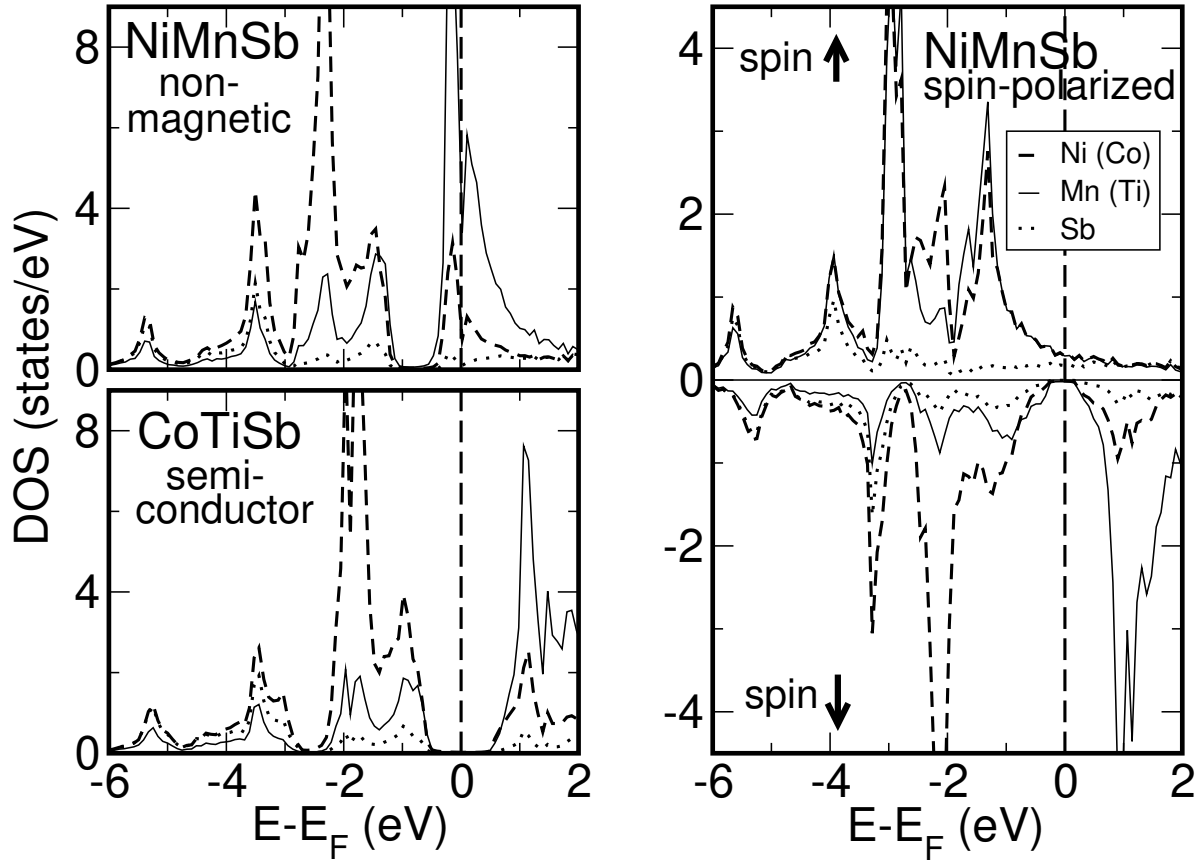


Figure 3. Atom-resolved density of states (DOS) of NiMnSb for a paramagnetic (upper left) and ferromagnetic (right) calculation. In the left bottom panel the DOS for the semiconductor CoTiSb. The zero energy value corresponds to the Fermi level E_F .

Thus the Ni d -bands contain a bonding Mn d admixture, while the higher Mn d -bands are antibonding hybrids with small Ni d -admixtures. Similarly, the Sb p -bands exhibit strong Ni d - and somewhat smaller Mn d -contributions.

This configuration for NiMnSb is energetically not stable, since (i) the Fermi energy lies in the middle of an antibonding band and (ii) since the Mn atom can gain considerable exchange energy by forming a magnetic moment. Therefore the spin-polarized results (figure 3 right) show a considerably different picture. In the majority (spin \uparrow) band the Mn d states are shifted to lower energies and form a common d band with the Ni d states, while in the minority band (spin \downarrow) the Mn states are shifted to higher energies and are unoccupied, so that a band gap at E_F is formed separating the occupied d bonding from the unoccupied d -type antibonding states. Thus NiMnSb is a half-metal, with a band gap at E_F in the minority band and a metallic sp -like DOS at E_F in the majority band. The total magnetic moment per unit cell, located mostly at the Mn atom, can be easily estimated to be exactly $4 \mu_B$. Note that NiMnSb has 22 valence electrons per unit cell, 10 from Ni, 7 from Mn and 5 from Sb. Since, due to the gap at E_F , in the minority band exactly 9 bands are fully occupied (1 Sb-like s band, 3

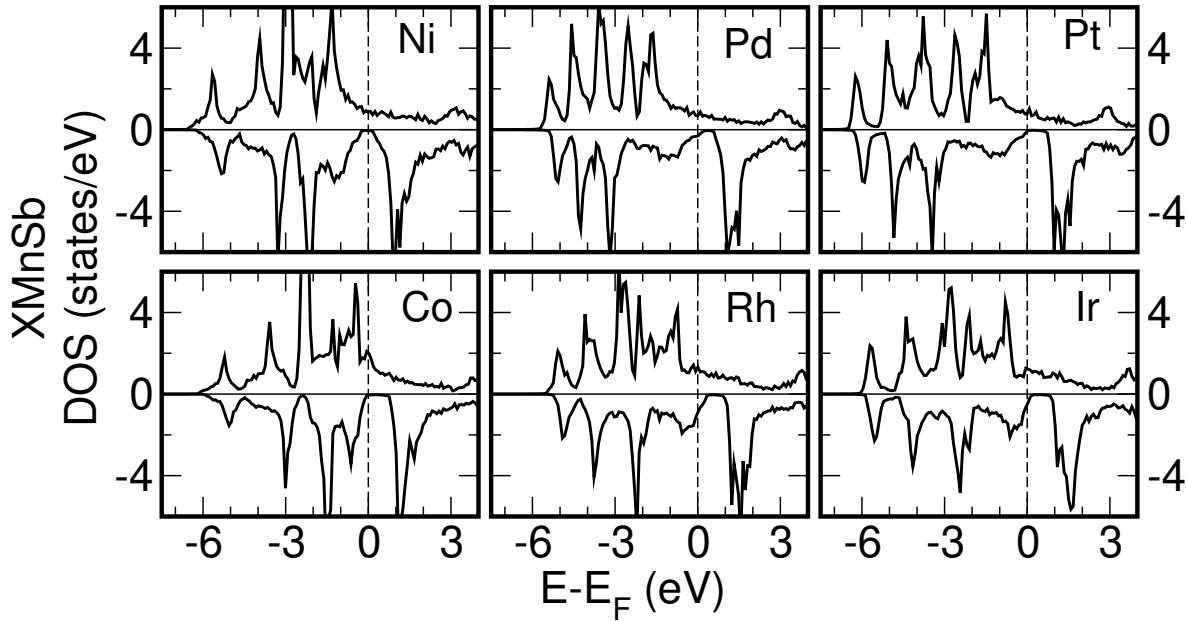


Figure 4. DOS of XMnSb compounds for $X = \text{Ni}, \text{Pd}, \text{Pt}$ and $\text{Co}, \text{Rh}, \text{Pd}$

Sb-like p bands and 5 Ni-like d bands) and accommodate 9 electrons per unit cell, the majority band contains $22 - 9 = 13$ electrons, resulting in the moment of $4 \mu_B$ per unit cell.

The above non-spinpolarized calculation for NiMnSb (figure 3 left upper panel) suggests, that if we could shift the Fermi energy as in a rigid band model, a particular stable compound would be obtained if the Fermi level falls for both spin directions into the band gap. Then for both spin directions 9 bands would be occupied, resulting in a semiconducting Heusler alloys indeed exist. As a typical example, figure 3 shows also the DOS of CoTiSb, which has a gap of 0.82 eV [7]. The gap is indirect corresponding to transitions from the valence band maximum at Γ to the conduction band minimum at X . Other such semiconductors are CoZrSb (0.83 eV), FeVSb (0.36 eV) and NiTiSn (0.14 eV), where the values in the bracket denote the size of the gap [7].

The band structure of the minority states of the half-Heusler alloys is most important for the understanding of the magnetic properties, and this band structure is basically universally valid for all half-Heusler alloys including the above semiconductors. This can be seen, for example, in the work of Nanda and Dasgupta who studied the band structure of the half-Heusler semiconductor FeVSb [33]. There, a “fat band representation” was used, with the plotted widths of the bands indicating the weight of the local orbitals to the band eigenstates. It was shown that around the band gap the eigenstates are dominated by the Fe and V d states which strongly hybridise with each other, with the Fe weights being stronger in the valence d band and the V states in the conduction band. The analogous feature can also be seen in the local density of states in figure 3. Below the five Fe d bands are the three Sb p bands which have also

Table 1. Calculated spin magnetic moments in μ_B for the XMnSb compounds. (The experimental lattice constants [4] have been used.) The deviations from integral total moment for the half-metallic compounds are due to numerical angular momentum cutoff (see text).

$m^{spin}(\mu_B)$	X	Mn	Sb	Void	Total	Half-metallic
NiMnSb	0.264	3.705	-0.060	0.052	3.960	yes
PdMnSb	0.080	4.010	-0.110	0.037	4.017	no
PtMnSb	0.092	3.889	-0.081	0.039	3.938	no
CoMnSb	-0.132	3.176	-0.098	0.011	2.956	yes
RhMnSb	-0.134	3.565	-0.144	<0.001	3.287	no
IrMnSb	-0.192	3.332	-0.114	-0.003	3.022	no
FeMnSb	-0.702	2.715	-0.053	0.019	1.979	yes

small contributions of Fe and V states. Analogously the Fe and V bands have small contributions of Sb p states (and even smaller contributions from the Sb s states). The V t_{2g} and e_g states exhibit a small crystal field splitting of 0.7 eV, with the e_g level being lower due to their weaker hybridisation with the Fe e_g states in tetrahedral symmetry, while for the Fe states this splitting is negligible. Most important is, that the gap arises from the hybridisation of the Fe and the V states and that the Sb p states are very deep and do not affect the gap.

Table 1 summarises the calculated magnetic moments for a series of XMnSb-type half-Heusler alloys. The calculations of the density of states show that NiMnSb, CoMnSb and FeMnSb are half-metals, *i.e.*, the Fermi level is in the minority gap, while for PtMnSb, PdMnSb and IrMnSb E_F enters slightly and for RhMnSb more strongly into the valence band, reducing the spin polarization.

The total magnetic moment in μ_B is just the difference between the number of occupied spin-up states and occupied spin-down states. The number of spin-down bands below the gap is in all cases $N_\downarrow = 9$. Ignoring for a moment the small penetration of E_F into the valence band for some of these compounds, we directly deduce the number $N_\uparrow = Z_t - N_\downarrow = Z_t - 9$ of occupied spin-up states and the moment, $M = (N_\uparrow - N_\downarrow) \mu_B = (Z_t - 2 \times N_\downarrow) \mu_B = (Z_t - 18) \mu_B$ from the total number of valence electrons, Z_t . We then find $N_\uparrow = 13$ and $M = 4 \mu_B$ for NiMnSb and for the isovalent compounds with Pd and Pt, $N_\uparrow = 12$ and $M = 3 \mu_B$ for CoMnSb, RhMnSb and IrMnSb, and $N_\uparrow = 11$ and $M = 2 \mu_B$ for FeMnSb, provided that the Fermi level stays within the gap. Penetration of E_F into the valence band for PtMnSb, PdMnSb, IrMnSb, and RhMnSb causes a deviation of M from the integral values.

The *ab-initio* calculated local moment per unit cell as given in table 1 is close to 4 μ_B in the case of NiMnSb, PdMnSb and PtMnSb, which is in agreement with the half-metallic character (or nearly half-metallic character in the case of PdMnSb) observed in the calculations. Note that due to the angular momentum cutoff the KKR method can only give the correct integer number 4, if Lloyd's formula is used in the evaluation

of the integrated density of states [34], which is not the case in the present calculations. We also find that the local moment of Mn is not far away from the total number of $4 \mu_B$ although there are significant (positive) contributions from the X-atoms and a negative contribution from the Sb atom. The antiferromagnetic coupling between the Sb and Mn moments is due to the different behavior of the p bands created by the Sb atoms, discussed in the next section. The minority p bands are more located within the Wigner-Seitz cell of Sb. On the other hand the majority p bands are more expanded in space and contain a larger Mn d -admixture and thus the total Sb spin moment has a negative sign.

We also find that for the half-metallic CoMnSb and IrMnSb compounds the total moment is about $3 \mu_B$. Here, the local moment of Mn is higher than the total moment by at most $0.5 \mu_B$. The reduction of the total moment to $3 \mu_B$ is therefore accompanied by negative Co and Ir spin moments, *i.e.*, these atoms couple antiferromagnetically to the Mn moments. The hybridization between Co and Mn is considerably larger than between Ni and Mn, and is a consequence of the smaller electronegativity difference and the larger extent of the Co orbitals. Therefore the minority valence band of CoMnSb has a larger Mn admixture than the one of NiMnSb whereas the minority conduction band of CoMnSb has a larger Co admixture than the Ni admixture in the NiMnSb conduction band, while the populations of the majority bands are barely changed. As a consequence, the Mn moment is reduced by the increasing hybridization, while the Co moment becomes negative, resulting finally in a reduction of the total moment from 4 to $3 \mu_B$. Table 1 also shows that substitution of Co with Fe leads again to a half-metallic alloy with a total spin moment of $2 \mu_B$ as has been already shown by de Groot *et al.* in reference [35].

2.2. Origin of the Gap

The local DOS shown in figure 3 for the ferromagnet NiMnSb and for the semiconductor CoTiSb show that the DOS close to the gap is dominated by d -states: in the valence band by bonding hybrids with large Ni or Co admixture and in the conduction band by the antibonding hybrids with large Mn or Ti admixture. Thus the gap originates from the strong hybridization between the d states of the two transition metal atoms. This is sketched schematically in figure 5. In this respect the origin of the gap is similar to the gap in compound semiconductors like GaAs which is enforced by the hybridization of the lower lying As sp -states with the energetically higher Ga sp -states. Note that in the C1_b-structure the Ni and Mn sublattices form a zinc-blende structure, which is important for the formation of the gap. The difference with respect to GaAs is then that 5 d -orbitals, *i.e.* 3 t_{2g} and 2 e_g orbitals, are involved in the hybridization, instead of 4 sp^3 -hybrids in the compound semiconductors.

Giving these arguments it is tempting to claim, that also a hypothetical zinc-blende compound like NiMn or PtMn should show a half-metallic character with a gap at E_F in the minority band. Figure 6 shows the results of a self-consistent calculation for such

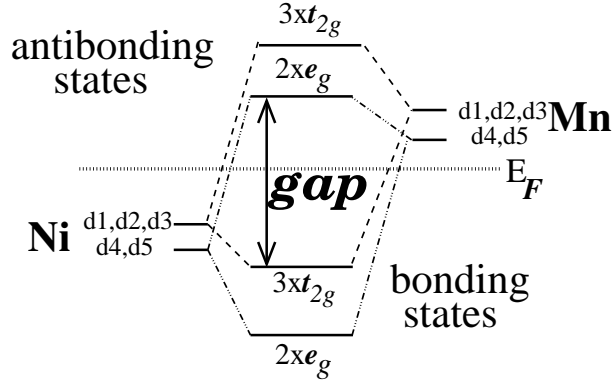


Figure 5. Schematic illustration of the origin of the gap in the minority band in half-Heusler alloys and semiconductors: The energy levels E_b of the energetically lower lying bonding hybrids are separated from the levels E_{ab} of the antibonding hybrids by a gap, such that only the bonding states are occupied. Due to legibility reasons, we use d1, d2 and d3 to denote the d_{xy} , d_{yx} and d_{zx} t_{2g} -orbitals, respectively, and d4, d5 for the d_{z^2} , $d_{x^2-y^2}$ e_g -orbitals.

zinc-blende NiMn and PtMn, with the same lattice constant as NiMnSb. Indeed a gap is formed in the minority band. In the hypothetical NiMn the Fermi energy is slightly above the gap, however the isoelectronic PtMn compound shows nearly half-metallicity. In this case the occupied minority states consist of six bands, a low-lying s -band and five bonding d -bands, both of mostly Pt character. Since the total number of valence electrons is 17, the majority bands contain 11 electrons, so that the total moment per unit cell is $11 - 6 = 5\mu_B$, which is indeed obtained in the calculations. This is the largest possible moment for this compound, since in the minority band all 5 Mn d -states are empty while all majority d -states are occupied. The same limit of $5\mu_B$ is also the maximal possible moment of the half-metallic $C1_b$ Heusler alloys.

The gap in the half-metallic $C1_b$ compounds is normally indirect, with the maximum of the valence band at the Γ point and the minimum of the conduction band at the X -point. For NiMnSb we obtain a band gap of about 0.5 eV, which is in good agreement with the experiments of Kirillova and collaborators [25], who, analyzing their infrared spectra, estimated a gap width of ~ 0.4 eV. As seen already from figure 4 the gap of CoMnSb is considerable larger (~ 1 eV) and the Fermi level is located at the edge of the minority valence band.

As it is well-known, the local density approximation (LDA) and the generalized gradient approximation (GGA) strongly underestimate the values of the gaps in semiconductors, typically by a factor of two. However, very good values for these gaps are obtained in the so-called GW approximation of Hedin and Lundqvist [36], which describes the screening in semiconductors very well. On the other hand the minority gap in the half-metallic systems might be better described by the LDA and GGA since in these systems the screening is metallic.

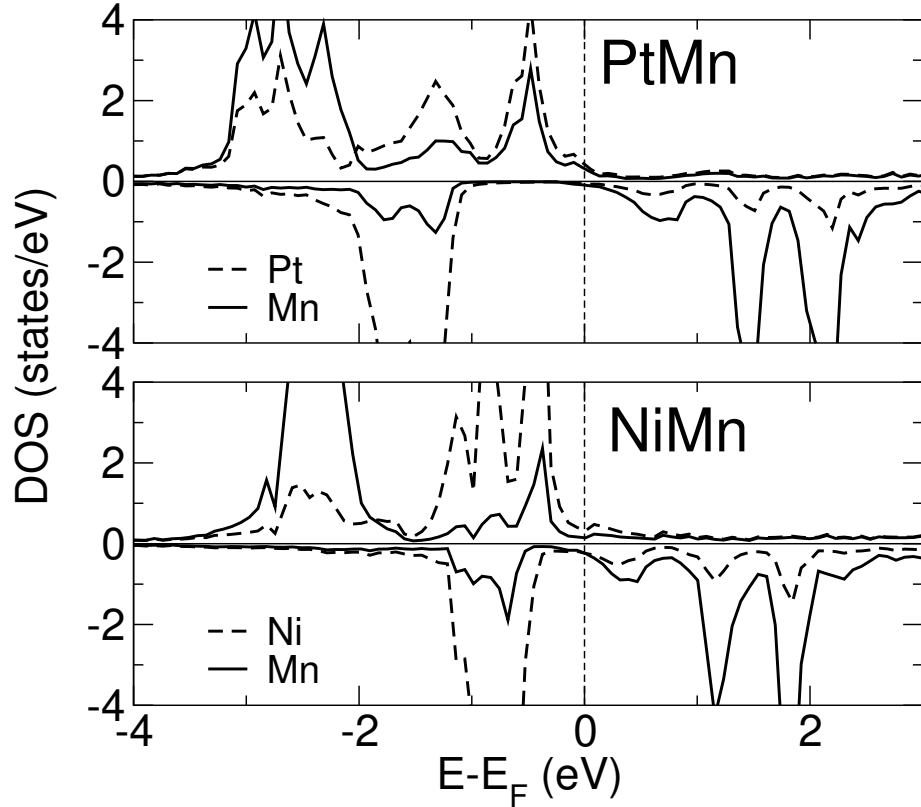


Figure 6. Atom-resolved DOS for the hypothetical PtMn and NiMn crystallizing in the zinc-blende structure.

2.3. Role of *sp*-Elements

While the *sp*-elements are not responsible for the existence of the minority gap, they are nevertheless very important for the physical properties of the Heusler alloys and the structural stability of the $C1_b$ structure, as we discuss in the following. There are three important features:

(i) While an Sb atom has 5 valence electrons ($5s^2, 5p^3$), in the NiMnSb compound each Sb atom introduces a deep lying *s*-band, at about -12 eV, and three *p*-bands below the center of the *d*-bands. These bands accommodate a total of 8 electrons per unit cell, so that formally Sb acts as a triple charged Sb^{3-} ion. Analogously, a Te-atom behaves in these compounds as a Te^{2-} ion and a Sn-atom as a Sn^{4-} ion. This does not mean, that locally such a large charge transfer exists. In fact, the *s*- and *p*-states strongly hybridize with the TM *d*-states and the charge in these bands is delocalized and locally Sb even loses about one electron, if one counts the charge in the Wigner-Seitz cells. What counts here is that the *s*- and *p*-bands accommodate 8 electrons per unit cell, thus effectively reducing the *d*-charge of the TM atoms.

This is nicely illustrated by the existence of the semiconducting compounds CoTiSb and NiTiSn. Compared to CoTiSb, in NiTiSn the missing *p*-charge of the Sn atom is replaced by an increased *d* charge of the Ni atom, so that in both cases all 9 valence bands are occupied.

(ii) The *sp*-atom is very important for the structural stability of the Heusler alloys. For instance, it is difficult to imagine that the calculated half-metallic NiMn and PtMn alloys with zinc-blende structure, the LDOS of which are shown in figure 6, actually exist, since metallic alloys prefer highly coordinated structures like fcc, bcc, hcp etc. Therefore the *sp*-elements are decisive for the stability of the $C1_b$ compounds. A careful discussion of the bonding in these compounds has been recently published by Nanda and Dasgupta [37] using the crystal orbital Hamiltonian population (COHP) method. For the semiconductor FeVSb they find that, while the largest contribution to the bonding arises from the V-*d* – Fe-*d* hybridization, contributions of similar size arise also from the Fe-*d* – Sb-*p* and the V-*d* – Sb-*p* hybridization. Similar results are also valid for the semiconductors like CoTiSb and NiTiSn and in particular for the half-metal NiMnSb. Since the majority *d*-band is completely filled, the major part of the bonding arises from the minority band, so that similar arguments as for the semiconductors apply.

(iii) Another property of the *sp*-elements is worthwhile mentioning: substituting the Sb atom in NiMnSb by Sn, In or Te destroys the half-metallicity [38]. This is in contrast to the substitution of Ni by Co or Fe, which is documented in table 1. The total moment of $4 \mu_B$ for NiMnSb is reduced to $3 \mu_B$ in CoMnSb and $2 \mu_B$ in FeMnSb, thus preserving half-metallicity. In NiMnSn the total moment is reduced only to $3.3 \mu_B$ (instead of 3) and in NiMnTe the total moment increases only to $4.7 \mu_B$ (instead of 5). Thus by changing only the *sp*-element it is rather difficult to preserve the half-metallicity, since the density of states changes more like in a rigid band model [38].

2.4. Slater-Pauling Behavior

As discussed above the total moment of the half-metallic $C1_b$ Heusler alloys follows the simple rule: $M_t = Z_t - 18$, where Z_t is the total number of valence electrons per unit cell. In short, the total number of electrons Z_t is given by the sum of the number of spin-up and spin-down electrons, while the total moment M_t per unit cell is given by the difference

$$Z_t = N_\uparrow + N_\downarrow , \quad M_t = N_\uparrow - N_\downarrow \quad \rightarrow \quad M_t = Z_t - 2N_\downarrow \quad (1)$$

Since 9 minority bands are fully occupied, we obtain the simple "rule of 18" for half-metallicity in $C1_b$ Heusler alloys

$$M_t = Z_t - 18 \quad (2)$$

the importance of which has been recently pointed out by Jung et al. [39] and Galanakis et al. [38]. It is a direct analogue to the well-known Slater-Pauling behavior of the binary transition metal alloys [40]. The difference with respect to these alloys is, that in the half-Heusler alloys the minority population is fixed to 9, so that the screening is achieved by filling the majority band, while in the transition metal alloys the majority band is filled with 5 *d*-states and charge neutrality is achieved by filling the minority states. Therefore in the TM alloys the total moment is given by $M_t = 10 - Z_t$. Similar

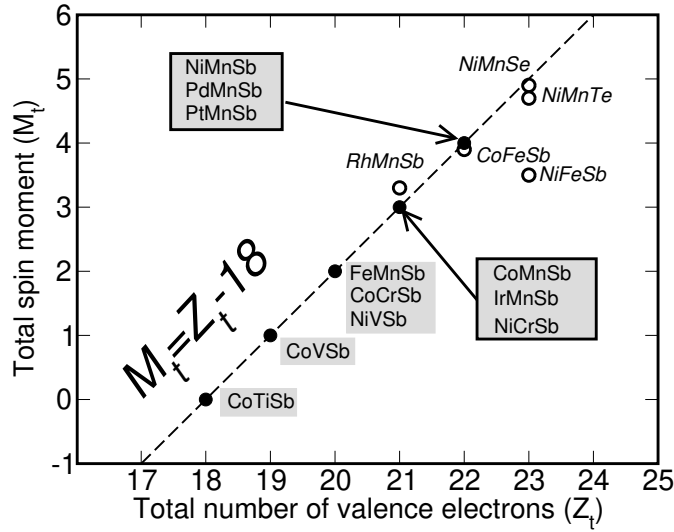


Figure 7. Calculated total spin moment per unit cell as a function of the total Z_t of valence electrons per unit cell for all the studied half Heusler alloys. The dashed line represents the Slater-Pauling behavior. With open circles we present the compounds deviating from the SP curve. Some experimental values for bulk systems near the SP curve from reference [4]: NiMnSb $3.85 \mu_B$, PdMnSb $3.95 \mu_B$, PtMnSb $4.14 \mu_B$ and finally CoTiSb non-magnetic.

rules with integer total moments are also valid for other half-metals, e.g. for the full-Heusler alloys like Co_2MnGe with $L2_1$ structure. For these alloys we will in section 3 derive the “rule of 24”: $M_t = Z_t - 24$, with arises from the fact that the minority band contains 12 electrons. For the half-metallic zinc-blende compounds like CrAs the rule is: $M_t = Z_t - 8$, since the minority As-like valence bands accommodate 4 electrons [13]. In all cases the moments are integer.

In figure 7 we have gathered the calculated total spin magnetic moments for the half-Heusler alloys which we have plotted as a function of the total number of valence electrons. The dashed line represents the rule $M_t = Z_t - 18$ obeyed by these compounds. The total moment M_t is an integer quantity, assuming the values 0, 1, 2, 3, 4 and 5 if $Z_t \geq 18$. The value 0 corresponds to the semiconducting phase and the value 5 to the maximal moment when all 5 majority d -states are filled. Firstly we varied the valence of the lower-valent (*i.e.* magnetic) transition metal atom. Thus we substitute V, Cr and Fe for Mn in the NiMnSb and CoMnSb compounds using the experimental lattice constants of the two Mn compounds. For all these compounds we find that the total spin moment scales accurately with the total charge and that they all present the half-metallicity.

As a next test we have substituted Fe for Mn in CoMnSb and NiMnSb, but both CoFeSb and NiFeSb lose their half-metallic character. In the case of NiFeSb the majority d -states are already fully occupied as in NiMnSb, thus the additional electron has to be screened by the minority d -states, so that the Fermi level falls into the minority Fe states and the half-metallicity is lost; for half-metallicity a total moment of $5 \mu_B$ would be required which is clearly not possible. For CoFeSb the situation is more delicate. This

system has 22 valence electrons and if it would be a half-metal, it should have a total spin-moment of $4 \mu_B$ as NiMnSb. In reality our calculations indicate that the Fermi level is slightly above the gap and the total spin-moment is slightly smaller than $4 \mu_B$. The Fe atom possesses a comparable spin-moment in both NiFeSb and CoFeSb compounds contrary to the behavior of the V, Cr and Mn atoms. Except NiFeSb other possible compounds with 23 valence electrons are NiMnTe and NiMnSe. We have calculated their magnetic properties using the lattice constant of NiMnSb. As shown in figure 7, NiMnSe almost makes the $5 \mu_B$ (its total spin moment is $4.86 \mu_B$) and is nearly half-metallic, while its isovalent, NiMnTe, has a slightly smaller spin moment. NiMnSe and NiMnTe show big changes in the majority band compared to systems with 22 valence electrons as NiMnSb or NiMnAs, since antibonding p - d states, which are usually above E_F , are shifted below the Fermi level, thus increasing the total moment to nearly $5 \mu_B$.

3. Full Heusler Alloys

3.1. Electronic Structure of Co_2MnZ with $Z = Al, Si, Ga, Ge$ and Sn

The second family of Heusler alloys, which we discuss, are the full-Heusler alloys. We consider in particular compounds containing Co and Mn, as these are the full-Heusler alloys that have attracted most of the attention. They are all strong ferromagnets with high Curie temperatures (above 600 K) and (except Co_2MnAl) they show very little disorder [4]. They adopt the $L2_1$ structure shown in figure 2. Each Mn or sp atom, sitting in an octahedral symmetry position, has eight Co atoms as first neighbors, while each Co has four Mn and four sp atoms as first neighbors and thus the symmetry of the crystal is reduced to the tetrahedral one. The Co atoms occupying the two different sublattices are chemically equivalent as the environment of the one sublattice is the same as the environment of the second one rotated by 90° . Although in the $L2_1$ structure, the Co atoms are sitting on second neighbor positions, their interaction is important to explain the magnetic properties of these compounds as we will show in the next section.

In figure 8 we show the spin-resolved density of states for the Co_2MnAl , Co_2MnGa , Co_2MnSi and Co_2MnGe compounds calculated using the FSKKR. Firstly as shown by photoemission experiments by Brown *et al.* in the case of Co_2MnSn [41] and verified by our calculations, the valence band extends around 6 eV below the Fermi level and the spin-up DOS shows a large peak just below the Fermi level for these compounds. Ishida *et al.* [42] predicted them to be half-metals with small spin-down gaps ranging from 0.1 to 0.3 eV depending on the material. Although our previous calculations showed a very small DOS at the Fermi level, in agreement with the ASW results of Kübler *et al.* [40] for Co_2MnAl and Co_2MnSn , a recalculation of our KKR results with a higher ℓ -cut-off of $\ell_{\max} = 4$ restores the gap and we obtain good agreement with the recent results of Picozzi *et al.* [43] obtained using the FLAPW method. The gap is indirect, with the maximum of the valence band at Γ and the minimum of the conduction band at the X -point.

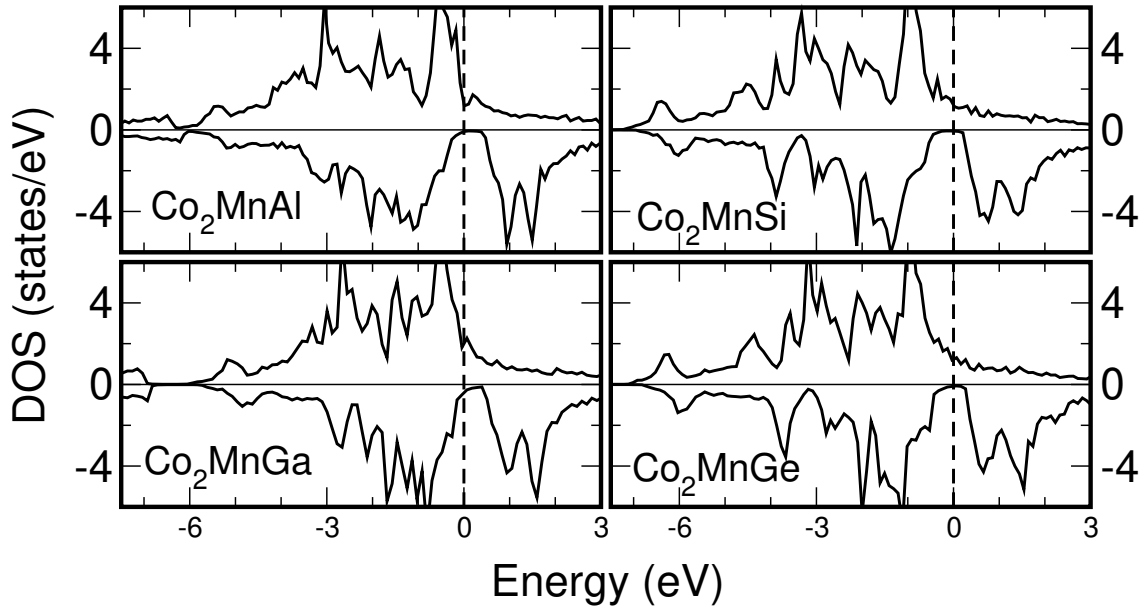


Figure 8. Atom-resolved DOS for the Co_2MnZ compounds with $\text{Z} = \text{Al, Si, Ge, Sn}$ compounds

In table 2 we have gathered the atom-resolved and total moments of the Co_2MnZ compounds. In the case of the half-Heusler alloys like NiMnSb the Mn spin moment is very localized due to the exclusion of the spin-down electrons at the Mn site and amounts to about $3.7 \mu_B$ in the case of NiMnSb ; in CoMnSb the increased hybridization between the Co and Mn spin-down electrons decreased the Mn spin moment to about $3.2 \mu_B$. In the case of the full-Heusler alloys each Mn atom has eight Co atoms as first neighbors instead of four as in CoMnSb , and this stronger hybridization is very important reducing the Mn spin moment even further to less than $3 \mu_B$, except in the case of Co_2MnSn where it is comparable to the CoMnSb compound. The Co atoms are ferromagnetically coupled to the Mn spin moments and they possess a spin moment that varies from ~ 0.7 to $1.0 \mu_B$. Note that in the half-metallic $C1_b$ Heusler alloys, the X -atom has a very small moment only, in the case of CoMnSb the Co moment is even negative. However, in the full Heusler alloys the Co moment is large and positive and arises basically from two unoccupied Co bands in the minority conduction band, as explained below. Therefore both Co atoms together can have a moment of about $2 \mu_B$, if all majority Co states are occupied. This is basically the case for Co_2MnSi , Co_2MnGe and Co_2MnSn (see table 2). In contrast to this, the sp atom has a very small negative moment which is one order of magnitude smaller than the Co moment. The negative sign of the induced sp moment characterizes most of the studied full and half Heusler alloys with very few exceptions. The compounds containing Al and Ga have 28 valence electrons and the ones containing Si, Ge and Sn 29 valence electrons. The former compounds have a total spin moment of $4\mu_B$ and the latter ones of $5\mu_B$, in agreement with the experimentally deduced moments of these compounds [44]. So it seems that the total spin moment, M_t , is related to the total number of valence electrons, Z_t , by the simple relation: $M_t = Z_t - 24$, while in the

Table 2. Calculated spin magnetic moments per unit cell in μ_B for the Co_2MnZ compounds, where Z stands for the sp atom. (The experimental lattice constants [4] have been used.) The deviations from integral total moment for the half-metallic compounds are due to numerical angular momentum cutoff (see text). All compounds are half-metallic.

$m^{spin}(\mu_B)$	Co	Mn	Z	Total
Co_2MnAl	0.768	2.530	-0.096	3.970
Co_2MnGa	0.688	2.775	-0.093	4.058
Co_2MnSi	1.021	2.971	-0.074	4.940
Co_2MnGe	0.981	3.040	-0.061	4.941
Co_2MnSn	0.929	3.203	-0.078	4.984

half-Heusler alloys the total magnetic moment is given by the relation $M_t = Z_t - 18$. In the following section we will analyze the origin of this rule.

3.2. Origin of the gap in Full-Heusler Alloys

Similar to the half-Heusler alloys, the four sp -bands are located far below the Fermi level and are thus irrelevant for the gap. Therefore, we consider only the hybridization of the 15 d states of the Mn atom and the two Co atoms. For simplicity we consider only the d -states at the Γ point, which show the full structural symmetry. We will give here a qualitative picture; for a thorough group theoretical analysis, see reference [45].

Firstly we note that the Co atoms form a simple cubic lattice and that the Mn atoms (and the Ge atoms) occupy the body centered sites and have 8 Co atoms as nearest neighbors. Although the distance between the Co atoms is a second neighbor distance, the hybridization between these atoms is qualitatively very important. Therefore we start with the hybridization between these Co atoms which is qualitatively sketched in figure 9. The 5 d -orbitals are divided into the twofold degenerate d_{z^2} , $d_{x^2-y^2}$ (e_g) and the threefold degenerate d_{xy} , d_{yz} , d_{zx} (t_{2g}) states. The e_g orbitals (t_{2g} orbitals) of each atom can only couple with the e_g orbitals (t_{2g} orbitals) of the other Co atom forming bonding hybrids, denoted by e_g (or t_{2g}) and antibonding orbitals, denoted by e_u (or t_{1u}). The coefficients in front of the orbitals give the degeneracy. Since the Co atoms form a simple cubic lattice with each Co atom surrounded by 6 other Co atoms, the crystal field splitting is such that $E_{e_g} > E_{t_{2g}}$.

In a second step we consider the hybridization of these Co-Co orbitals with the Mn d -orbitals. As we show in the right-hand part of figure 9, the doubly degenerated e_g orbitals hybridize with the d_{z^2} and $d_{x^2-y^2}$ of the Mn that transform according to the same representation. They create a doubly degenerate bonding e_g state that is very low in energy and an antibonding one that is unoccupied and above the Fermi level. The $3 \times t_{2g}$ Co orbitals couple to the $d_{xy,yz,zx}$ of the Mn and create 6 new orbitals, 3 of which are bonding and occupied and the other three are antibonding and high in energy. Since each Co atom sits in the center of a Mn tetrahedron, the crystal field splitting

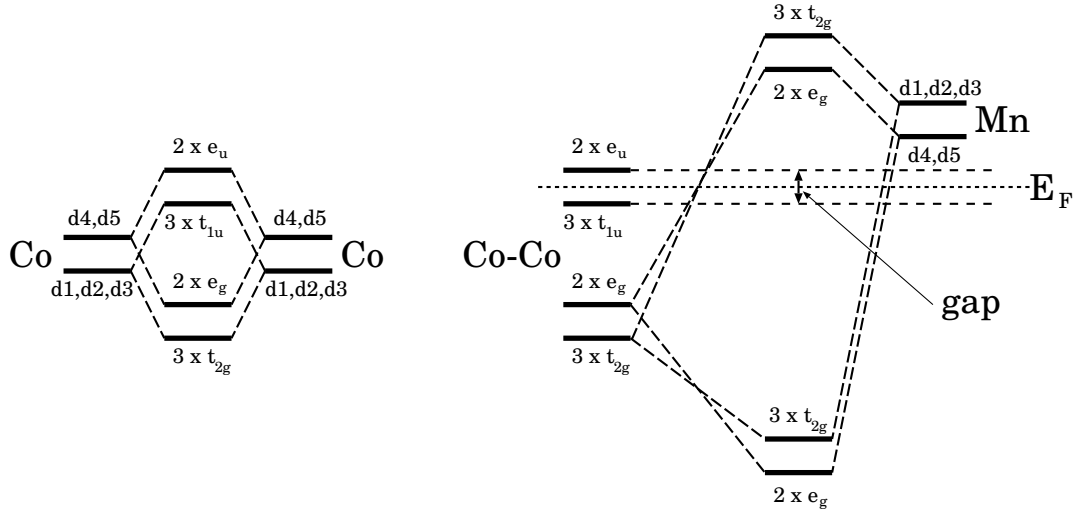


Figure 9. Schematic illustration of the origin of the gap in the minority band in full-Heusler alloys. Due to legibility reasons, we use d1, d2 and d3 to denote the d_{xy} , d_{yz} and d_{zx} orbitals, respectively, and d4, d5 for the d_{z^2} , $d_{x^2-y^2}$ orbitals.

of the bonding and antibonding states is such that $E_{e_g} < E_{t_{2g}}$. Finally the $2 \times e_u$ and $3 \times t_{1u}$ Co orbitals *can not* couple with any of the Mn d-orbitals since none of these is transforming according to the *u* representations and since they are orthogonal to the Co e_u and t_{1u} states. With respect to the Mn and the Ge atoms these states are therefore non-bonding. The t_{1u} states are below the Fermi level and they are occupied, while the e_u are just above the Fermi level. Thus, due to lack of hybridisation with the Mn states, the octahedral crystal field splitting $E_{e_u} > E_{t_{1u}}$ survives. In summary, in total 8 minority d-bands are filled and 7 are empty.

Therefore, all 5 Co-Mn bonding bands are occupied and all 5 Co-Mn antibonding bands are empty, and the Fermi level falls in-between the 5 non-bonding Co bands, such that the three lower-lying t_{1u} bands are occupied and the two e_u bands are empty. The maximal moment of the full Heusler alloys is therefore $7 \mu_B$ per unit cell, which would be achieved, if all majority d-states were occupied.

In order to demonstrate the existence of the t_{1u} and e_u states at the Fermi level, we show in figure 10 the LDOS of Co_2MnGe at the Co and Mn sites, which are splitted up into the local d_{xy} , d_{yz} and d_{zx} orbitals (normally referred to as t_{2g} ; full lines) and the local d_{z^2} and $d_{x^2-y^2}$ orbitals (normally e_g ; dashed). In the nomenclature used above, the d_{xy} , d_{yz} and d_{zx} contributions contain both the t_{2g} and the t_{1u} contributions, while the d_{z^2} and $d_{x^2-y^2}$ orbitals contain the e_g and e_u contributions. The Mn DOS clearly shows a much bigger effective gap at E_F , considerably larger than in CoMnSb (figure 4), as one would expect from the stronger hybridization in Co_2MnGe . However, the real gap is determined by the Co-Co interaction only, in fact by the $t_{1u} - e_u$ splitting, and is smaller than in CoMnSb . Thus the origin of the gap in the full-Heusler alloys is rather subtle.

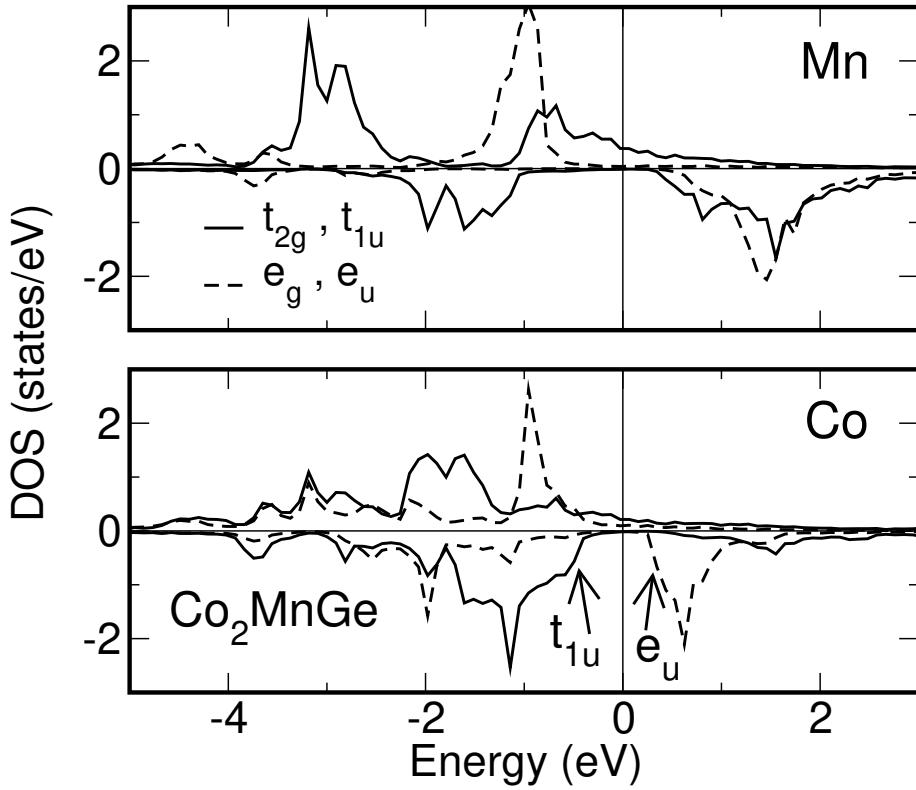


Figure 10. Atom- and symmetry-resolved DOS for the Co_2MnGe compound.

3.3. Slater-Pauling (SP) behavior of the Full-Heusler alloys

Following the above discussion we investigate the Slater-Pauling behavior. In figure 11 we have plotted the total spin moments for all the compounds under study as a function of the total number of valence electrons. The dashed line represents the half-metallicity rule of the full Heusler alloys: $M_t = Z_t - 24$. This rule arises from the fact that the minority band contains 12 electrons per unit cell: 4 are occupying the low lying s and p bands of the sp element and 8 the Co-like minority d bands ($2 \times e_g$, $3 \times t_{2g}$ and $3 \times t_{1u}$), as explained above (see figure 9). Since 7 minority bands ($2 \times \text{Co } e_u$, $5 \times \text{Mn } d$) are unoccupied, the largest possible moment is $7 \mu_B$ and occurs when all majority d -states are occupied.

Overall we see that many of our results coincide with the Slater-Pauling curve. Some of the Rh compounds show small deviations which are more serious for the Co_2TiAl compound. We see that there is no compound with a total spin moment of $7 \mu_B$ or even $6 \mu_B$. Moreover, we show examples of half-metallic materials with less than 24 electrons, namely Mn_2VGe with 23 valence electrons and Mn_2VAl with 22 valence electrons. Firstly, we have calculated the spin moments of the compounds Co_2YAl where $\text{Y} = \text{Ti, V, Cr, Mn and Fe}$. The compounds containing V, Cr and Mn show a similar behavior. As we substitute Cr for Mn, we depopulate one spin-up state and thus the spin moment of Cr is around $1 \mu_B$ smaller than the Mn one while the Co moments are practically the same for both compounds. Substituting V for Cr has a larger effect since

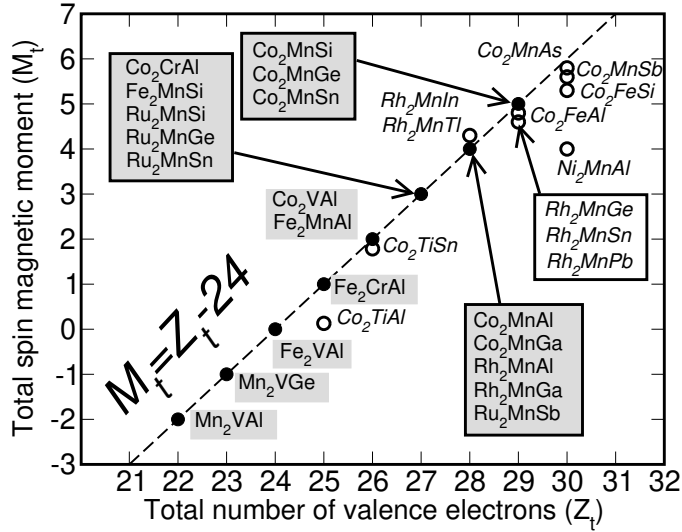


Figure 11. Calculated total spin moments for all the studied full Heusler alloys. The dashed line represents the Slater-Pauling behavior. With open circles we present the compounds deviating from the SP curve. Some experimental values for bulk systems near the SP curve from reference [4]: Co_2MnAl $4.01 \mu_B$, Co_2MnSi $5.07 \mu_B$, Co_2MnGa $4.05 \mu_B$, Co_2MnGe $5.11 \mu_B$, Co_2MnSn $5.08 \mu_B$, Co_2FeSi $5.9 \mu_B$, Mn_2VAI $-1.82 \mu_B$ and finally Fe_2VAI non-magnetic.

also the Co spin-up DOS changes slightly and the Co magnetic moment is increased by about $0.1 \mu_B$ compared to the other two compounds and V possesses a small moment of $0.2 \mu_B$. This change in the behavior is due to the smaller hybridization between the Co and V atomic states as compared to the Cr and Mn ones. Although all three Co_2VAI , Co_2CrAl and Co_2MnAl compounds are on the SP curve as can be seen in figure 11, this is not the case for the compounds containing Fe and Ti. If the substitution of Fe for Mn followed the same logic as the one of Cr for Mn then the Fe moment should be around $3.5 \mu_B$ which is a very large moment for the Fe site. Therefore it is energetically more favorable for the system that also the Co moment is increased, as was also the case for the other systems with 29 electrons like Co_2MnSi , but while the latter one makes it to $5 \mu_B$, Co_2FeAl reaches a value of $4.9 \mu_B$. In the case of Co_2TiAl , it is energetically more favorable to have a weak ferromagnet than an integer moment of $1 \mu_B$ as it is very difficult to magnetize the Ti atom. Even in the case of the Co_2TiSn the calculated total spin magnetic moment of $1.78 \mu_B$ (compared to the experimental value of $1.96 \mu_B$ [46]) arises only from the Co atoms as was also shown experimentally by Pendel *et al.* [47], and the Ti atom is practically nonmagnetic and the latter compound fails to follow the SP curve.

As a second family of materials we have studied the compounds containing Fe. Fe_2VAI has in total 24 valence electrons and is a semi-metal, *i.e.* nonmagnetic with a very small DOS at the Fermi level, as is already known experimentally [48]. All the studied Fe compounds follow the SP behavior as can be seen in figure 11. In the case of the Fe_2CrAl and Fe_2MnAl compounds the Cr and Mn atoms have spin moments

comparable to the Co compounds and similar DOS. In order to follow the SP curve the Fe in Fe_2CrAl is practically nonmagnetic while in Fe_2MnAl it has a small negative moment. When we substitute Si for Al in Fe_2MnAl , the extra electron exclusively populates Fe spin-up states and the spin moment of each Fe atom is increased by $0.5 \mu_B$ contrary to the corresponding Co compounds where also the Mn spin moment was considerably increased. Finally we calculated as a test Mn_2VAl and Mn_2VGe that have 22 and 23 valence electrons, respectively, to see if we can reproduce the SP behavior for compounds with less than 24 electrons. As we have already shown, Fe_2VAl is nonmagnetic and Co_2VAl , which has two electrons more, has a spin moment of $2 \mu_B$. Mn_2VAl has two valence electrons less than Fe_2VAl and its total spin moment is $-2\mu_B$ and thus it follows the SP behavior; negative total spin moment means that the “minority” band with the gap has more occupied states than the “majority” one.

As we have already mentioned the maximal moment of a full-Heusler alloy is seven μ_B , and should occur, when all 15 majority d states are occupied. Analogously for a half-Heusler alloy the maximal moment is $5 \mu_B$. However this limit is difficult to achieve, since due to the hybridization of the d states with empty sp -states of the transition metal atoms (sites X and Y in figure 2), d -intensity is transferred into states high above E_F , which are very difficult to occupy. Although in the case of half-Heusler alloys, we could identify systems with a moment of nearly $5 \mu_B$, the hybridization is much stronger in the full-Heusler alloys so that a total moment of $7 \mu_B$ seems impossible. Therefore we restrict our search to possible systems with $6 \mu_B$, *i.e.* systems with 30 valence electrons, but as shown also in figure 11, none of them makes the $6 \mu_B$ exactly. Co_2MnAs shows the largest spin moment: $5.8 \mu_B$. The basic reason why moments of $6 \mu_B$ are so difficult to achieve, is that as a result of the strong hybridization with the two Co atoms the Mn atom cannot have a much larger moment than $3 \mu_B$. While due to the empty e_u -states the two Co atoms have no problem to contribute a total of $2 \mu_B$, the Mn moment is hybridization-limited.

4. Effect of the Lattice Parameter

In this section we will study the influence of the lattice parameter on the electronic and magnetic properties of the $C1_b$ and $L2_1$ Heusler alloys. To the best of our knowledge no relevant experimental study exists. For this reason we plot in figure 12 the DOS of NiMnSb and CoMnSb for the experimental lattice parameter and the ones compressed and expanded by 2 %. First one sees, that upon compression the Fermi level moves in the direction of the conduction band, upon expansion towards the valence band. In both cases, however, the half-metallic character is conserved. To explain this behavior, we first note that the Fermi level is determined by the metallic DOS in the majority band. As we believe, the shift of E_F is determined by the behavior of the Sb p -states, in particular by the large extension of these states as compared to the d states. Upon compression the p -states are squeezed and hybridize stronger, thus pushing the d -states and the Fermi level to higher energies, *i.e.* towards the minority conduction band. In

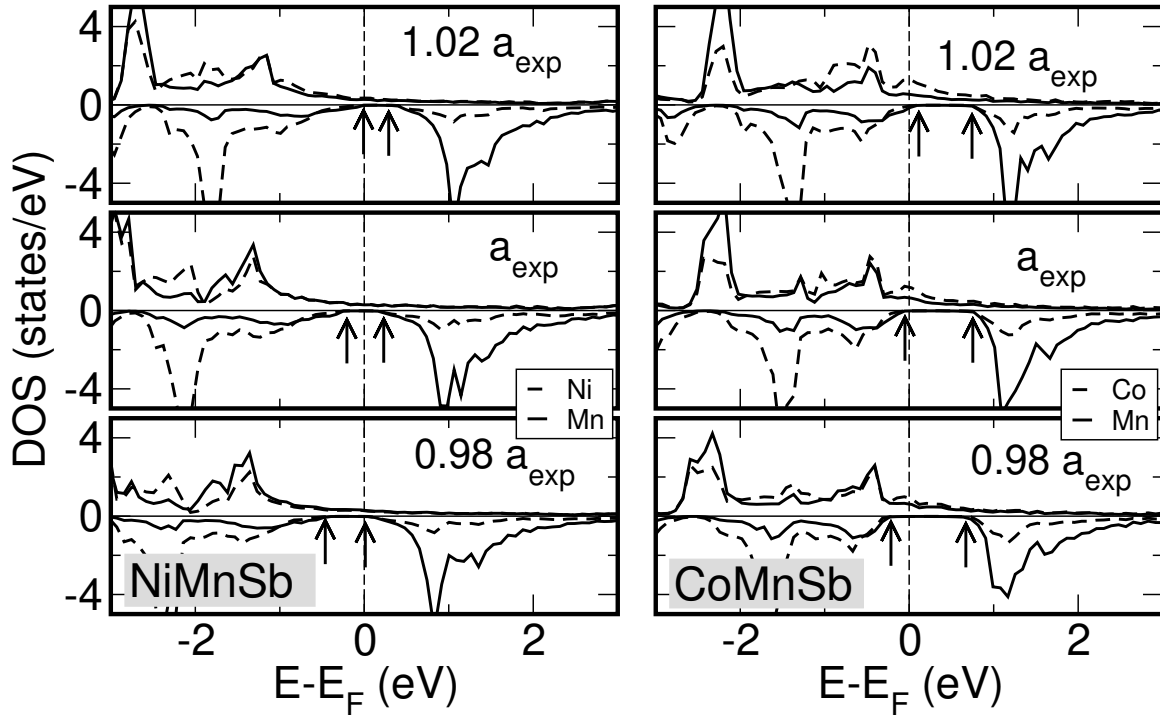


Figure 12. Atom-resolved DOS for the experimental lattice parameter for NiMnSb and CoMnSb, compared with the once compressed or expanded by 2%. With the small arrow we denote the edges of the minority gap.

addition the Mn d and Ni or Co d states hybridize stronger, which increases the size of the gap. Upon expansion the opposite effects are observed. In the case of NiMnSb and for the experimental lattice constant the gap-width is ~ 0.4 eV. When the lattice is expanded by 2% the gap shrinks to 0.25 eV and when compressed by 2% the gap-width is increased to 0.5 eV. Similarly in the case of CoMnSb, the gap is 0.8 eV for the experimental lattice constant, 0.65 for the 2% expansion and 0.9 eV for the case of the 2% compression.

For the full-Heusler alloys the pressure dependence has been recently studied by Picozzi et al. [43] for Co_2MnSi , Co_2MnGe and Co_2MnSn , using both the LDA and the somewhat more accurate GGA. The general trends are similar: the minority gap increases with compression, and the Fermi level moves in the direction of the conduction band. For example in the case of Co_2MnSi the gap-width is 0.81 eV for the theoretical equilibrium lattice constant of 10.565 Å. When the lattice constant is compressed to ~ 10.15 Å, the gap-width increases to about 1 eV. Results by Picozzi et al. [43] of are shown in figure 13.

The calculations show that for the considered changes of the lattice constants of $\pm 2\%$, half-metallicity is preserved. There can be sizeable changes of the local moments, but the total moment remains constant, since E_F stays in the gap.

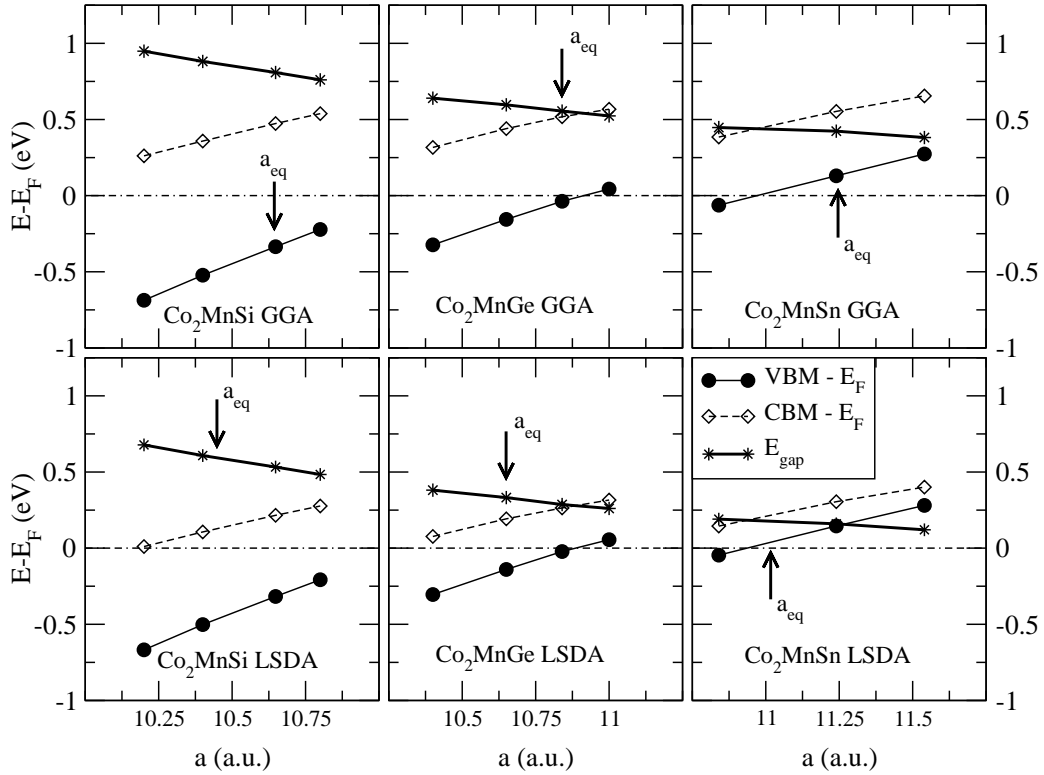


Figure 13. Position of the conduction band maximum (CBM) and valence band minimum (VBM) relative to the Fermi level for Co_2MnSi , Co_2MnGe , and Co_2MnSn , calculated for a range of lattice parameters within the LSDA and the GGA. The gap width is also shown. The calculated equilibrium lattice parameter is indicated by a_{eq} . (Figure redrawn after Picozzi et al. [43].)

5. Effect of spin-orbit coupling (SOC)

The calculations presented up to this point have neglected the spin-orbit coupling (SOC). Intuitively, however, one expects that SOC can be of crucial importance for the half-metallic property: In the presence of SOC, the electron spin is no more a good quantum number, so that the electron eigenfunctions cannot conserve their spin degree of freedom. Wavefunctions within the half-metallic gap must then have partly spin-down character. As a result, the celebrated half-metallic gap cannot really be 100% there even at $T \rightarrow 0$. In materials where the SOC is weak, the DOS within the “gap” is expected to be low, and the polarization close to, but not exactly at, 100% [49, 50]. Another result of SOC is the appearance of orbital magnetic moment. This, too, is weak in Heusler alloys with low SOC strength.

5.1. Polarization in the gap in the presence of SOC

We begin our discussion with the effect of SOC on the polarization within the half-metallic gap, where by the term “gap” we understand the energy region where the spin-down DOS is zero if we neglect the spin-orbit coupling, and very small if we take

it into account. The natural theoretical framework to approach the spin-orbit coupling is the Dirac equation, where relativistic effects are inherent. Nevertheless it is more instructive to include SOC as a perturbation in the Schrödinger Hamiltonian, starting from the unperturbed two-spin-channel description. The perturbation connecting the two spin channels reads, in terms of the Pauli matrices $\vec{\sigma}$ and the orbital momentum \vec{L} :

$$V_{\text{so}}(r) = \frac{1}{2m^2c^2} \frac{\hbar}{2r} \frac{1}{r} \frac{dV}{dr} \vec{L} \cdot \vec{\sigma} = \begin{pmatrix} V_{\text{so}}^{\uparrow\uparrow} & V_{\text{so}}^{\uparrow\downarrow} \\ V_{\text{so}}^{\downarrow\uparrow} & V_{\text{so}}^{\downarrow\downarrow} \end{pmatrix}. \quad (3)$$

Here, $V(r)$ is the unperturbed one-electron potential at an atomic site, and is assumed to be spherically symmetric. Deviations from the spherical symmetry arise only close to the interstitial region between atoms, where the contribution to the spin-orbit interaction is anyhow small. The 2×2 matrix is the perturbation expressed in spinor basis, demonstrating the non-diagonal terms $V_{\text{so}}^{\uparrow\downarrow}$ and $V_{\text{so}}^{\downarrow\uparrow}$ which are responsible for spin-flip processes; \uparrow and \downarrow denote the spin up and spin down direction. Thus, if we denote the unperturbed hamiltonian for the two spin directions by $H^{0\uparrow}$ and $H^{0\downarrow}$, and the unperturbed Bloch eigenfunctions as $\Psi_{n\vec{k}}^{0\uparrow}$ and $\Psi_{n\vec{k}}^{0\downarrow}$, then the Schrödinger equation for the perturbed wavefunction $\Psi_{n\vec{k}} = (\Psi_{n\vec{k}}^{\uparrow}, \Psi_{n\vec{k}}^{\downarrow})$ has the form

$$\begin{pmatrix} H^{0\uparrow} + V_{\text{so}}^{\uparrow\uparrow} - E & V_{\text{so}}^{\uparrow\downarrow} \\ V_{\text{so}}^{\downarrow\uparrow} & H^{0\downarrow} + V_{\text{so}}^{\downarrow\downarrow} - E \end{pmatrix} \begin{pmatrix} \Psi_{n\vec{k}}^{\uparrow} \\ \Psi_{n\vec{k}}^{\downarrow} \end{pmatrix} = 0. \quad (4)$$

When E is within the half-metallic band gap, the unperturbed spin-down solution $\Psi_{n\vec{k}}^{0\downarrow}$ vanishes, and only the spin-up solution $\Psi_{n\vec{k}}^{0\uparrow}$ is present. Acting with the perturbed hamiltonian of Eq. (4) on the unperturbed spinor $(\Psi_{n\vec{k}}^{0\uparrow}, 0)$ gives us a formal solution for the first-order correction to the spin-down wavefunction:

$$\Psi_{n\vec{k}}^{(1)\downarrow} = -\frac{1}{H^{0\downarrow} + V_{\text{so}}^{\downarrow\downarrow} - E_{n\vec{k}}^{0\uparrow}} V_{\text{so}}^{\downarrow\uparrow} \Psi_{n\vec{k}}^{0\uparrow} \quad (5)$$

where $E_{n\vec{k}}^{0\uparrow} (= E)$ is the energy eigenvalue corresponding to the state $\Psi_{n\vec{k}}^{0\uparrow}$. This result shows that, within the gap, the spin-down intensity is a weak image of the band structure $E_{n\vec{k}}^{0\uparrow}$ of the spin-up band. Since the spin-down density of states $n_{\downarrow}(E)$ is related to $|\Psi_{n\vec{k}}^{(1)\downarrow}|^2$, we expect in the gap region a quadratic dependence of $n_{\downarrow}(E)$ on the spin-orbit coupling strength: $n_{\downarrow}(E) \sim (V_{\text{so}}^{\downarrow\uparrow})^2$. Furthermore, the term $-1/(H^{0\downarrow} + V_{\text{so}}^{\downarrow\downarrow} - E_{n\vec{k}}^{0\uparrow})$ (this is actually the Green function) increases the weight of the spin-down states near the \vec{k} points where the unperturbed spin-up and spin-down bands cross, *i.e.*, $E_{n\vec{k}}^{0\uparrow} = E_{n'\vec{k}}^{0\downarrow}$. To see this we can rewrite Eq. (5) by expanding the Green function in spectral representation:

$$\begin{aligned} \Psi_{n\vec{k}}^{(1)\downarrow}(\vec{r}) &= \int d^3r' \sum_{n'} \frac{\Psi_{n'\vec{k}}^{(0)\downarrow}(\vec{r}) \Psi_{n'\vec{k}}^{(0)\downarrow*}(\vec{r}')}{E_{n\vec{k}}^{0\uparrow} - E_{n'\vec{k}}^{0\downarrow}} V_{\text{so}}^{\downarrow\uparrow}(\vec{r}') \Psi_{n\vec{k}}^{(0)\uparrow}(\vec{r}') \\ &= \sum_{n'} \frac{\langle \Psi_{n'\vec{k}}^{0\downarrow} | V_{\text{so}}^{\downarrow\uparrow} | \Psi_{n\vec{k}}^{0\uparrow} \rangle}{E_{n\vec{k}}^{0\uparrow} - E_{n'\vec{k}}^{0\downarrow}} \Psi_{n'\vec{k}}^{0\downarrow}(\vec{r}) \end{aligned} \quad (6)$$

Here, the summation runs only over the band index n' and not over the Bloch vectors \vec{k}' , because Bloch functions with $\vec{k}' \neq \vec{k}$ are mutually orthogonal. Close to the crossing

point $E_{n\vec{k}}^{0\uparrow} - E_{n'\vec{k}}^{0\downarrow}$ the denominator becomes small and the bands strongly couple. Then one should also consider higher orders in the perturbation expansion. Such a band crossing can occur at the gap edges, since within the gap itself there are no spin-down solutions. Therefore, a blow-up of $n_\downarrow(E)$ is expected near the gap edges (but still within the gap).

The spin polarization $P(E)$ at an energy E (and in particular at E_F) is related to the spin-dependent DOS via the expression

$$P = \frac{n_\uparrow(E_F) - n_\downarrow(E_F)}{n_\uparrow(E_F) + n_\downarrow(E_F)} \quad (7)$$

$$\approx 1 - 2 n_\downarrow(E_F)/n_\uparrow(E_F) \quad \text{for small } n_\downarrow/n_\uparrow .$$

In Refs. [49, 50], $P(E_F)$ was calculated for a number of half-Heusler alloys and other half-metals. The calculations were done within density-functional theory, utilising the KKR Green function method. The approach was fully relativistic, solving the Dirac equation rather than treating the spin-orbit coupling as a perturbation. Nevertheless the qualitative behavior which was described above was revealed. Table 3 summarises the results for $P(E_F)$ and for the polarization in the middle of the gap, $P(E_M)$, for the half-Heusler alloys. The trend is that alloys which include heavier elements show a lower spin polarization. This becomes most evident by inspection of the values of $P(E_M)$, since for some of the alloys the Fermi level approaches or enters the valence band, so that $P(E_F)$ does not always reflect the SOC strength. In particular, NiMnSb shows a high value for $P(E_M)$ (99.3%), which decreases when we substitute the 3d element Ni with the heavier, 4d element, Pd, and even more so when we substitute it with the even heavier, 5d element, Pt. This effect is only expected, since it is well-known that heavier elements show in general a stronger SOC. As an extreme case, the hypothetical alloy MnBi, which was found to be half-metallic in the zinc-blende structure if one ignores the spin-orbit interaction [51], is found to have a value of $P(E_F) = 77\%$ [50] when SOC is accounted for (here, the 6p wavefunctions of Bi are responsible for the strength of the effect). As a conclusion, the spin-orbit coupling reduces $P(E_F)$, but the resulting values are still high. Nevertheless, we point out that calculations on half-metallic ferromagnets containing heavy elements (*e.g.*, lanthanides) should take into account the spin-orbit coupling for a reliable quantitative result.

5.2. Orbital moments in Heusler alloys

The orbital moments in Heusler alloys are expected to be small. This is a result of the cubic symmetry, of the fact that the magnetic transition elements here are relatively light (3d series) and of the metallic nature of the electronic states.

Orbital moments for Heusler compounds were calculated by Picozzi *et al.* [43] for Co_2MnSi , -Ge, and -Sn, and more systematically by Galanakis [52] for ten half-Heusler and nine full-Heusler compounds. These results are summarized in tables 4 and 5. As expected, the values of the orbital moments m_{orb} (calculated within the LSDA) are small. It is known that the LSDA can underestimate m_{orb} by up to 50%, but the trends

Table 3. Calculated spin polarisation P at the Fermi level (E_F) and in the middle of the spin-down gap (E_M), and ratio of spin-down/spin-up DOS in the middle of the gap ($n_\downarrow/n_\uparrow(E_M)$), for various half-Heusler alloys. The alloys PdMnSb and PtMnSb present a spin-down gap, but are not half-metallic, as E_F is slightly below the gap.

Compound	$P(E_F)$	$P(E_M)$	$(n_\downarrow/n_\uparrow)(E_M)$
CoMnSb	99.0%	99.5%	0.25%
FeMnSb	99.3%	99.4%	0.30%
NiMnSb	99.3%	99.3%	0.35%
PdMnSb	40.0%	98.5%	0.75%
PtMnSb	66.5%	94.5%	2.70%

Table 4. Spin (m_{spin}) and orbital (m_{orbit}) magnetic moments in μ_B for the XMnSb half-Heusler compounds. The last three columns are the total spin and orbital magnetic moment and their sum, respectively

Alloy	MnSb-based half-Heusler alloys								
	m_{spin}^X	m_{orbit}^X	m_{spin}^{Mn}	m_{orbit}^{Mn}	m_{spin}^{Sb}	m_{orbit}^{Sb}	$m_{\text{spin}}^{\text{total}}$	$m_{\text{orbit}}^{\text{total}}$	m^{total}
FeMnSb	-0.973	-0.060	2.943	0.034	-0.040	-0.002	1.958	-0.028	1.930
CoMnSb	-0.159	-0.041	3.201	0.032	-0.101	-0.001	2.959	-0.010	2.949
NiMnSb	0.245	0.015	3.720	0.027	-0.071	-0.001	3.951	0.040	3.991
CuMnSb	0.132	0.006	4.106	0.032	0.028	-0.006	4.335	0.032	4.367
RhMnSb	-0.136	-0.033	3.627	0.035	-0.141	-0	3.360	0.001	3.361
PdMnSb	0.067	0.007	4.036	0.028	-0.117	-0	4.027	0.035	4.062
AgMnSb	0.106	0.006	4.334	0.031	0.040	-0.007	4.556	0.029	4.585
IrMnSb	-0.201	-0.094	3.431	0.092	-0.109	-0.001	3.130	-0.004	3.126
PtMnSb	0.066	0.006	3.911	0.057	-0.086	0	3.934	0.063	3.997
AuMnSb	0.134	0.021	4.335	0.027	0.056	-0.006	4.606	0.044	4.650

are considered reliable. The highest orbital moment, almost $0.1 \mu_B$, appears at the Ir and Mn atoms in IrMnSb, but with opposite signs for the two atoms, so that the total m_{orb} is close to zero (note that also the Ir spin moment is opposite to the Mn spin moment; for Ir in this compound we obtain a ratio of $m_{\text{orb}}/m_{\text{spin}} \simeq 1/2$).

6. Summary and Outlook

We have reviewed the electronic structure and the magnetic properties of spin-gap Heusler alloys. Although Heusler alloys are complex systems, calculations based on local density-functional theory followed by a careful analysis allow reveal the basic mechanisms for the formation of the gap, as well as the correlation between valence charge and spin moment, being reflected in the Slater-Pauling behavior.

The d - d hybridization between the transition atoms composing Heusler alloys is essential for the formation of the gap at E_F . In the case of half-Heusler alloys (*e.g.*,

Table 5. Spin (m_{spin}) and orbital (m_{orbit}) magnetic moments in μ_B for the X_2YZ full-Heusler compounds. The last three columns are the total spin and orbital magnetic moments and their sum, respectively

Alloy	Half-metallic full-Heusler alloys								
	m_{spin}^X	m_{orbit}^X	m_{spin}^Y	m_{orbit}^Y	m_{spin}^Z	m_{orbit}^Z	$m_{\text{spin}}^{\text{total}}$	$m_{\text{orbit}}^{\text{total}}$	m^{total}
Co ₂ MnAl	0.745	0.012	2.599	0.013	-0.091	-0	3.998	0.038	4.036
Co ₂ MnSi	0.994	0.029	3.022	0.017	-0.078	0.001	4.932	0.076	5.008
Co ₂ MnGe	0.950	0.030	3.095	0.020	-0.065	0.001	4.931	0.081	5.012
Co ₂ MnSn	0.905	0.038	3.257	0.025	-0.079	0	4.988	0.101	5.089
Co ₂ CrAl	0.702	0.012	1.644	0.008	-0.082	0	2.966	0.033	2.999
Co ₂ FeAl	1.094	0.045	2.753	0.060	-0.095	-0	4.847	0.149	4.996
Fe ₂ MnAl	-0.311	-0.015	2.633	0.014	-0.016	0.001	1.994	-0.014	1.980
Mn ₂ VAL	-1.398	-0.034	0.785	-0.009	0.013	0.005	-1.998	-0.073	-2.071
Rh ₂ MnAl	0.304	-0.011	3.431	0.034	-0.037	-0.001	4.002	0.011	4.013

NiMnSb) the gap is created by the hybridization and bonding-antibonding splitting between the Mn d and the Ni d states. In the case of full-Heusler alloys (*e.g.*, Co₂MnSi) the gap originates hybridization of the d states of the two Co atoms and the subsequent interaction of these hybrids with the Mn d states. At this stage, the sp atom is a spectator; nevertheless, due to its electronegativity it acts as a hole reservoir, contributing to a shift of the spin-up bands and therefore to the value of the total spin moment. Due to the different exchange splitting of the different atoms in the unit cell, the hybridization of spin-up states does not show the same pattern as for the spin-down states. Thus, in the end, a gap appears only among the spin-down bands, while for spin-up a metallic character arises.

When the systems are half-metallic, a Slater-Pauling behavior connects the spin moment M_t per unit cell to the number of valence electrons Z_t per unit cell by $M_t = (Z_t - 18) \mu_B$ for half-Heusler alloys and by $M_t = (Z_t - 24) \mu_B$ for full-Heusler alloys. These “magic numbers” 18 and 24 (double the number of occupied spin-down valence states) are consequent of the number and position of the spin-down states after the d - d hybridizations have taken place. The common nature of the hybridizations among half- (and among full-) Heusler alloys leads to these Slater-Pauling rules.

While the formation of the gap by hybridization seems straightforward, the position of E_F with respect to the gap (and thus the half-metallic property itself) is sensitive to the lattice constant. Starting from a half-metallic state, compression (or expansion) of the lattice drives E_F higher into the conduction band (or lower into the valence band). Thus the half-metallic property, when present, is stable within 3-5% change of the lattice parameter.

The spin-orbit coupling seems to have small effect on the physical properties of these compounds. On the one hand, the spin polarization within the gap is reduced, but only by an amount of the order of one or two percent. On the other hand, the

orbital moments are small.

As an outlook we discuss the theoretical perspective of potential applications of half-metallic Heusler alloys in spintronics. There are two major issues: one concerning the interfaces of these materials with semiconductors, and one regarding the half-metallic behavior of these materials at elevated temperatures (since density-functional calculations reproduce ground-state properties). On the former subject, the results so-far are rather discouraging. *Ab-initio* calculations reveal the presence of interface states at almost all Heusler-semiconductor contacts. These states reduce or even invert the spin polarization at the interface, an effect which can be critical for applications [53]. The reason seems to be that, at the interface with the semiconductor, the *d-d* hybridization creating the gap stops abruptly. Further research is needed in this area in order to find material combinations where the hybridization will continue coherently across the interface and the gap will be preserved. Such cases are known to exist for contacts of other types of half-metals with semiconductors, *e.g.*, the half-metallic zinc-blende pnictides and chalcogenides [13].

On the question of elevated temperature, very little theoretical work has been done [54], due to the complexity that higher temperature introduces. The high Curie point of Heusler alloys, found both in experiment and theory [55], gives hope for applicability at room temperature. However, average magnetic order is not necessarily connected with the presence of a half-metallic gap at high temperatures. Especially due to their compound nature, Heusler alloys could have an extremely complex magnetic excitation spectrum (as is also indicated by experiments [56]), with the various sublattices exhibiting fluctuations different in nature and energy scale. Theoretical work in this direction is in progress and will be reported elsewhere [57].

Acknowledgements

We would like to thank Silvia Picozzi for useful discussions and for providing us with her results.

References

- [1] Žutić I, Fabian J and Das Sarma A 2004 *Rev. Mod. Phys.* **76** 323
- [2] Wolf S A, Awschalom D D, Buhrman R A, Daughton J M, von Molnár S, Roukes M L, Chtchelkanova A Y and Treger D M 2001 *Science* **294** 1488
- [3] Heusler F 1903 *Verh. Dtsch. Phys. Ges.* **5** 219
- [4] Webster P J and Ziebeck K R A, in *Alloys and Compounds of d-Elements with Main Group Elements. Part 2.*, edited by H.R.J. Wijn, Landolt-Börnstein, New Series, Group III, Vol. 19, Pt.c (Springer-Verlag, Berlin), pp. 75-184
- [5] Ziebeck K R A and Neumann K -U, in *Magnetic Properties of Metals*, edited by H. R. J. Wijn, Landolt-Börnstein, New Series, Group III, Vol. 32/c (Springer, Berlin), 2001, pp. 64-414
- [6] Pierre J, Skolozdra R V, Tobola J, Kaprzyk S, Hordequin C, Kouacou M A, Karla I, Currat R and Lelièvre-Berna E 1997 *J. Alloys Comp.* **262-263** 101
- [7] Tobola J, Pierre J, Kaprzyk S, Skolozdra R V and Kouacou M A 1998 *J. Phys.: Condens. Matter*

10 1013; Tobola J and Pierre J 2000 *J. Alloys Comp.* **296** 243; Tobola J, Kaprzyk S and Pecheur P 2003 *Phys. Status Solidi (b)* **236** 531

[8] Zayak A T, Entel P, Enkovaara J, Ayuela A, and Nieminen R M 2003 *Phys. Rev. B* **68**, 132402

[9] de Groot R A, Mueller F M, van Engen P G and Buschow K H J 1983 *Phys. Rev. Lett.* **50** 2024

[10] Soulé Jr R J, Byers J M, Osofsky M S, Nadgorny B, Ambrose T, Cheng S F, Broussard P R, Tanaka C T, Nowak J, Moodera J S, Barry A and Coey J M D 1998 *Science* **282** 85

[11] Kato H, Okuda T, Okimoto Y, Tomioka Y, Oikawa K, Kamiyama T, and Tokura T 2004 *Phys. Rev. B* **69**, 184412

[12] Shishidou T, Freeman A J, and Asahi R 2001 *Phys. Rev. B* **64**, 180401

[13] Galanakis I 2002 *Phys. Rev. B* **66** 012406; Galanakis I and Mavropoulos Ph 2003 *Phys. Rev. B* **67** 104417; Mavropoulos Ph, Galanakis I and Dederichs P H 2004 *J. Phys.: Condens. Matter* **16** 4261

[14] Sanvito S and Hill N A 2000 *Phys. Rev. B* **62**, 15553; Continenza A, Picozzi S, Geng W T, and Freeman A J 2001 *Phys. Rev. B* **64**, 085204; Liu B G 2003 *Phys. Rev. B* **67**, 172411; Sanyal B, Bergqvist L, and Eriksson O 2003 *Phys. Rev. B* **68**, 054417; Xie W-H, Liu B-G, and Pettifor D G 2003 *Phys. Rev. B* **68**, 134407; Xie W-H, Liu B-G, and Pettifor D G 2003 *Phys. Rev. Lett.* **91**, 037204; Xu Y Q, Liu B G, and Pettifor D G 2003 *Phys. Rev. B* **68**, 184435; Zhang M et al. 2003 *J. Phys.: Condens. Matter* **15**, 5017; Fong C Y, Qian M C, Pask J E, Yang L H, and Dag S 2004 *Appl. Phys. Lett.* **84**, 239; Pask J E, Yang L H, Fong C Y, Pickett W E, and Dag S 2003 *Phys. Rev. B* **67**, 224420; Zheng J-C and Davenport J W 2004 *Phys. Rev. B* **69**, 144415

[15] Akinaga H, Manago T, and Shirai M 2000 *Jpn. J. Appl. Phys.* **39**, L1118; Mizuguchi M, Akinaga H, Manago T, Ono K, Oshima M, and Shirai M 2002 *J. Magn. Magn. Mater.* **239**, 269; Mizuguchi M, Akinaga H, Manago T, Ono K, Oshima M, Shirai M, Yuri M, Lin H J, Hsieh H H, and Chen C T 2002 *J. Appl. Phys.* **91**, 7917; Mizuguchi M, Ono M K, Oshima M, Okabayashi J, Akinaga H, Manago T, and Shirai M 2002 *Surf. Rev. Lett.* **9**, 331; Nagao, Shirai M, and Miura Y 2004 *J. Appl. Phys.* **95**, 6518; Ono, Okabayashi J, Mizuguchi M, Oshima M, Fujimori A, and Akinaga H 2002 *J. Appl. Phys.* **91**, 8088; Shirai M 2001 *Physica E* **10**, 143; Shirai M 2003 *J. Appl. Phys.* **93**, 6844

[16] Zhao J H, Matsukura F, Takamura K, Abe E, Chiba D, and H. Ohno H 2001 *Appl. Phys. Lett.* **79**, 2776; Zhao J H, Matsukura F, Takamura K, Abe E, Chiba D, Ohno Y, Ohtani K, and Ohno H 2003 *Mat. Sci. Semicond. Proc.* **6**, 507

[17] Horne M, Strange P, Temmerman W M, Szotek Z, Svane A, and Winter H 2004 *J. Phys.: Condens. Matter* **16**, 5061

[18] Stroppa A, Picozzi S, Continenza A, and Freeman A J 2003 *Phys. Rev. B* **68**, 155203

[19] Akai H 1998 *Phys. Rev. Lett.* **81**, 3002

[20] Park J-H, Vescovo E, Kim H-J, Kwon C, Ramesh R, and Venkatesan T 1998 *Nature* **392**, 794

[21] Datta S and Das B 1990 *Appl. Phys. Lett.* **56**, 665

[22] Kilian K A and Victoria R H 2000 *J. Appl. Phys.* **87**, 7064

[23] Tanaka C T, Nowak J, and Moodera J S 1999 *J. Appl. Phys.* **86**, 6239

[24] Caballero J A, Park Y D, Childress J R, Bass J, Chiang W-C, Reilly A C, Pratt Jr. W P, and Petroff F 1998 *J. Vac. Sci. Technol. A* **16**, 1801; Hordequin C, Nozières J P, and Pierre J 1998 *J. Magn. Magn. Mater.* **183**, 225

[25] Kirillova M N, Makhnev A A, Shreder E I, Dyakina V P and Gorina N B 1995 *Phys. Status Solidi (b)* **187** 231

[26] Hanssen K E H M and Mijnarends P E 1990 *Phys. Rev. B* **34** 5009; Hanssen K E H M, Mijnarends P E, Rabou L P L M and K.H.J. Buschow K H J 1990 *Phys. Rev. B* **42** 1533

[27] Picozzi S, Continenza A and Freeman A J 2003 *J. Appl. Phys.* **94** 4723; Picozzi S, Continenza A and Freeman A J 2003 *J. Phys. Chem. Solids* **64** 1697

[28] Galanakis I 2004 *J. Phys.: Condens. Matter* **16** 8007; Galanakis I, Ležaić M, Bihlmayer G and Blügel S 2005 *Phys. Rev. B* **71**, 214431; Ležaić M, Galanakis I, Bihlmayer G, and Blügel S 2005 *J. Phys.: Condens. Matter* **17** 3121

- [29] Nagao K, Shirai M and Miura Y 2004 *J. Phys.: Condens. Matter* **16** S5725
- [30] Galanakis I and Dederichs P H (eds): Half-metallic alloys: fundamentals and applications, Springer Lecture notes in Physics vol. 676, Springer (2005).
- [31] Zeller R, Dederichs P H, Újfalussy B, Szunyogh L and Weinberger P 1995 *Phys. Rev. B* **52** 8807
- [32] Papanikolaou N, Zeller R and Dederichs P H 2002 *J. Phys.: Condens. Matter* **14** 2799
- [33] Nanda B R K and Dasgupta I 2003 *J. Phys.: Condens. Matter* **15**, 7307
- [34] Zeller R 2004 *J. Phys.: Condens. Matter* **16** 6453
- [35] de Groot R A, van der Kraan A M and Buschow K H J 1986 *J. Magn. Magn. Mater.* **61** 330
- [36] Hedin L and Lundqvist S 1969, In: Solid State Physics, vol 23, ed by F. Seitz, D. Turnbull, and H. Ehrenreich, (Academic Press, New York and London 1969) pp 1-181
- [37] Nanda B R K and Dasgupta S 2003 *J. Phys.: Condens. Matter* **15** 7307
- [38] Galanakis I, Dederichs P H and Papanikolaou N 2002 *Phys. Rev. B* **66** 134428
- [39] Jung D, Koo H J and Whangbo M J 2000 *J. Mol. Struct. (Theochem)* **527** 113
- [40] Kübler J 1984 *Physica B* **127** 257
- [41] D Brown, Crapper M D, Bedwell K H, Butterfield M T, Guilfoyle S J, Malins A E R and Petty M 1998 *Phys. Rev. B* **57** 1563
- [42] Ishida S, Akazawa S, Kubo Y and Ishida J 1982 *J. Phys. F: Met. Phys.* **12** 1111; Ishida S, Fujii S, Kashiwagi S and Asano S 1995 *J. Phys. Soc. Japan* **64** 2152
- [43] Picozzi S, Continenza A and Freeman A J 2002 *Phys. Rev. B* **66** 094421
- [44] Dunlap R A and Jones D F 1982 *Phys. Rev. B* **26** 6013; Plogmann S, Schlathölter T, Braun J, Neumann M, Yarmoshenko Yu M, Yablonskikh M V, Shreder E I, Kurmaev E Z, Wrona A and Ślebarski A 1999 *Phys. Rev.* **60** 6428
- [45] Galanakis I, Papanikolaou N and Dederichs P H 2002 *Phys. Rev. B* **66** 174429
- [46] van Engen P G, Buschow K H J and Erman M 1983 *J. Magn. Magn. Mater.* **30** 374
- [47] Pendl Jr W, Saxena R N, Carbonari A W, Mestnik Filho J and Schaff J 1996 *J. Phys.: Condens. Matter* **8** 11317
- [48] Feng Ye, Rhee J Y, Wiener T A, Lynch D W, Hubbard B E, Sievers A J, Schlagel D L, Lograsson T A, and Miller L L 2001 *Phys. Rev. B* **63**, 165109; Lue C S, Ross Jr. J H, Rathnayaka K D D, Naugle D G, Wu S Y and Li W-H 2001 *J. Phys.: Condens. Matter* **13**, 1585; Nishino Y, Kato H, Kato M, Mizutani U 2001 *Phys. Rev. B* **63**, 233303; A. Matsushita A, Naka T, Takanao Y, Takeuchi T, Shishido T, and Yamada Y 2002 *Phys. Rev. B* **65**, 075204
- [49] Mavropoulos Ph, Sato K, Zeller R, Dederichs P H, Popescu V and Ebert H 2004 *Phys. Rev. B* **69** 054424
- [50] Mavropoulos Ph, Galanakis I, Popescu V and Dederichs P H 2004 *J. Phys.: Condens. Matter* **16** S5759
- [51] Xu Y-Q, Liu B-G, and Pettifor D G 2002 *Phys. Rev. B* **66**, 184435
- [52] Galanakis I 2005 *Phys. Rev. B* **71** 012413
- [53] Mavropoulos Ph, Ležaić M, and Blügel S 2005 preprint: cond-mat/0506079
- [54] Dowben P A and Skomski R 2003 *J. Appl. Phys.* **93**, 7948
- [55] Sasioglu E, Sandratskii LM, Bruno P, and Galanakis I 2005 Accepted for publication in *Phys. Rev. B* (preprint: cond-mat/0507697)
- [56] Hordequin Ch, Pierre J, and Currat R 1996 *J. Magn. Magn. Mater.* **162**, 75
- [57] Ležaić M, Mavropoulos Ph, Enkovaara J, Bihlmayer G, and Blügel S 2005 (unpublished)